MATERIALS CHEMISTRY
FRONTIERS

CHINESE CHEMICAL SOCIETY

ROYAL SOCIETY OF CHEMISTRY

RESEARCH ARTICLE

View Article Online
View Journal

Cite this: DOI: 10.1039/d5qm00330j

Covalent organic framework-functionalized composites with high hydrophobicity to acids and bases for chemical protection

Junmei Li,[a] Zhixuan Duan,[a] Yinan Fan,[a] Ruigan Zhang,[a] Demao Ban,[a] Zhaolin Liu*[b] and Lifang Liu *[a]

Received 24th April 2025,
Accepted 7th July 2025

DOI: 10.1039/d5qm00330j

rsc.li/frontiers-materials

Public safety has been a long-term research focus. Improving the comprehensive properties of matrix materials is of great significance for chemical protection. However, a research gap exists in this field. In this study, a covalent organic framework (COF) was constructed using Benzene-1,3,5-tricarbaldehyde (TFB) and 2,3′-dimethyl-[1,1′-biphenyl] (BD(Me)$_2$) as building units, and a TFB-BD(Me)$_2$ COF was grown on Nomex nonwovens (NW) using vapor phase-assisted conversion. Based on their chemical protection mechanism, the prepared functional fabrics exhibited unique acid–base properties, high hydrophobicity, and excellent chemical stability. In addition, these functional fabrics, with good thermal stability, flame retardancy, and strength, enabled chemical protection in multiple scenarios. Overall, the simple and efficient preparation method makes these functional fabrics competitive in the field of chemical protective materials. At the same time, the use of COFs as a reinforcing material effectively broadens the application of COFs in chemical protection and lays a foundation for its exploration in other fields.

1. Introduction

Improving the comprehensive performance of fiber raw materials is a key issue in the development of new broad-spectrum long-lasting chemical-protective fabrics. At present, key technologies, such as structural modification[1] or functional modification,[2] are mostly used to improve the comprehensive performance of the base fabric. Covalent organic frameworks (COFs) are materials composed of periodic covalent bonds and interlayer interactions.[3] They are widely used in gas capture,[4,5] catalysis,[6,7] sensing,[8,9] energy storage,[10,11] drug delivery[12,13] and other fields. COFs possess the advantages of a large specific surface area, low density, good hydrophobicity, and good chemical stability and are expected to become improved materials that enhance the chemical protection performance of matrix materials.[14] However, as pure organic nanofillers, the preparation of COFs is limited by harsh synthetic conditions and powdered forms, which are difficult to generalize.[15] At present, the commonly used methods for preparing continuous COF base films include *in situ* growth,[16] layer-by-layer stacking,[17] and interfacial polymerization (IP).[18] For example, Yu *et al.*[19] prepared COF oligomers *via* homogeneous polymerization, and the resulting nanofiltration membranes exhibited organic solvent permeability, molecular selectivity and long-term stability. Khan *et al.*[20] prepared nanosheets through the dispersion of COFs as reactive fillers to yield mixed matrix membranes, which enhanced the rejection efficiency of salt solutions. At the same time, three-dimensional (3D) covalent organic framework (COF) crystals were introduced into different types of polymers to stimulate the interaction between the filler and the polymer, inducing the formation of COF-polymer junctions to improve the strength, ductility and toughness of the functional fabrics.[21] The synthesized COF-based composite membrane has strict requirements in terms of environmental conditions, preparation time, and device requirements. The emergence of vapor-assisted conversion (VAC) provides a new strategy for the synthesis of COFs.[22,23] The vapor-assisted conversion method has the characteristics of easy operation and wide adaptability of substrates and can be applied to a variety of textile materials. By precisely adjusting the proportion of precursors, the controllable growth of COFs on the fiber surface was realized, which broke through the limitations of the traditional preparation method with harsh conditions and a single product form, and successfully constructed a composite fabric with directional chemical protection function. This method significantly improves the protective properties of the fabrics while maintaining its original properties.

---

[a] *College of Textiles, Donghua University, Shanghai 201620, China. E-mail: lifangliu@dhu.edu.cn*

[b] *Hebei Textile and Garment Technology Innovation Center, Hebei University of Science and Technology, Shijiazhuang 050091, China. E-mail: liuzhaolin0508@163.com*

Nomex exhibits excellent high-temperature resistance, good dimensional stability, excellent spinnability, and chemical stability. It is widely used in aerospace,[25] building and construction,[26] air filtration,[27] personal protection,[24] and other fields. Most research studies have focused on utilizing COF-based materials to enhance the flame-retardant properties of Nomex. Shen *et al.*[28] designed a COF that was obtained by an indirect correlation between melamine and g-C_3N_4 as a flame-retardant coating. Under combustion, the flame retardant changes from a carbon layer to a thick honeycomb structure, preventing the dispersion of oxygen and combustible gases. Zhou *et al.*[29] used the unique microporous structure of COF as a low dielectric factor, combining it with a molecular design strategy to synthesize phosphonitrile-based COF-N functional fabrics, which exhibit excellent fire safety properties. However, Nomex itself does not have the properties of resistance to strong acids, strong alkalis, and some organic solvents, which limits its wide application in chemical protection.

In this study, Benzene-1,3,5-tricarboxybenzene (TFB) and 4,4′-diaminobiphenyl ($BD(Me)_2$) were used as building blocks; Nomex nonwovens (NW) were soaked in monomer solutions sequentially, and COFs were grown *in situ* on the substrate surface with the assistance of steam in a 1 : 1 ratio of trimethylbenzene and 1,4-dioxane, and finally, the NW-COF functional fabrics were obtained. By altering the COFs loading and water contact angle before and after, the chemical protection performance of the functional fabrics was further tested. It is notable that the optimized functional fabrics exhibit excellent performance, including hydrophobicity to superhydrophobicity, as well as competitive protection against various concentrations of salts, acids, and bases, and organic solutions. At the same time, the cycling stability test of the functional fabrics showed that NW had good compatibility with COF particles. The innovative combination of COFs and NW effectively compensates for the lack of chemical corrosion resistance of Nomex. This study provides a new direction for the broad-spectrum and long-term protection of chemical protective fabrics.

2. Experimental

2.1 Materials

All chemicals were commercial products and could be used directly without further purification. 1,4-Dioxane, dichloromethane (DCM), methanol, acetone, tetrahydrofuran (THF), and absolute ethanol were purchased from Sinopharm Group Co. Ltd (Shanghai, China). 1,3,5-Tricarboxybenzene (TFB), sodium hypochlorite (NaClO), and acetic acid (AcOH) were purchased from Titan Scientific Co. Ltd (Shanghai, China). 4,4′-Diaminobiphenyl ($BD(Me)_2$) was purchased from Rhawn Chemical Reagents Co., Ltd (Shanghai, China). Mesitylene was purchased from Aladdin Biochemical Technology Co., Ltd (Shanghai, China). Toluene was purchased from Lingfeng Chemical Reagent Co., Ltd (Shanghai, China). Methyl orange was purchased from Meiruier Biochemical Technology Co., Ltd (Shanghai, China). NW was made in the laboratory, with a thickness of 0.35 mm and mass of 40 g m^{-2}.

2.2 Preparation of TFB-$BD(Me)_2$ COF

0.1011 mmol of TFB and 0.1517 mmol of $BD(Me)_2$ were dissolved in 5 mL of trimethylbenzene and sonicated for 5 min to dissolve and form a homogeneous solution. Subsequently, the mixed solution was further sonicated for 5 min to ensure uniform dispersion of the monomers, and 6 M acetic acid solution (0.5 mL) was slowly added under agitation conditions. The reaction system was sealed, transferred to a 30 °C oil bath and the reaction was allowed to stand for 3 days. After the reaction was completed, the products were sequentially washed with xylene, DMF, and absolute ethanol, then centrifuged to collect the solids, and dried at 60 °C in vacuum for 6 h to finally obtain TFB-$BD(Me)_2$ COF.

2.3 Preparation of NW-COF functional fabrics

The surface was cleaned by sonicating the NW in absolute ethanol for 30 min, and then it was dried overnight in a 50 °C oven to complete the pretreatment. TFB (0.14 mmol) and $BD(Me)_2$ (0.21 mmol) were dissolved in 4 mL of trimethylbenzene and absolute ethanol, respectively, and sonicated with maximum power for 10 minutes to ensure uniform dispersion of the monomers. The 100 × 100 mm NW fabric was pre-wetted with acetic acid solution, and then immersed in the above monomer solution sequentially to evenly load the solution on the NW surface. Subsequently, the monomer-loaded NW was placed in a glass container containing 20 mL of a mixed solvent (medium ethylene and 1,4-dioxane, 1 : 1 v/v) sealed, and reacted in a 30 °C water bath for 24 h. After the reaction was complete, the functional fabric was sonicated in absolute ethanol for 4 min to remove the unreacted polymer, and then placed in a 30 °C vacuum oven to dry for 6 h. The preparation process is illustrated in Fig. 1. According to the different concentrations of the TFB monomer (0.02, 0.06, 0.1, 0.14, and 0.16 mmol), the resulting products were named VAC-0.02, VAC-0.06, VAC-0.1, VAC-0.14, and VAC-0.16, respectively.

2.4 Characterization

The scanning electron microscope (SEM) images were acquired by a FLEX 1000 SEM instrument (Hitachi USA). Fourier-transform infrared (FTIR) spectra were obtained using Spectrum Two (PerkinElmer, USA). X-ray photoelectron spectroscopy (XPS) was conducted using Escalab 250Xi (ThermoFisher Scientific, USA). X-ray diffraction (XRD) experiments were performed using a D/max-2550 PC instrument (Rigaku, Japan). Thermogravimetric analysis (TGA) was performed using TG209F1 (NETZSCH, Germany). N_2 was used as the test atmosphere. Brunner–Emmett–Teller (BET) measurements were performed using Autosorb iQ (Anton Paar American). The atomic force microscope (AFM) was obtained from Bruker (USA).

2.5 Breaking strength

The breaking strength properties of functional fabrics were tested on a YG026MB multi-functional electronic fabric strength machine (Wenzhou, China). The samples were cut to 300 × 100 mm. The tensile speed was set to (300 ± 10) mm min^{-1},

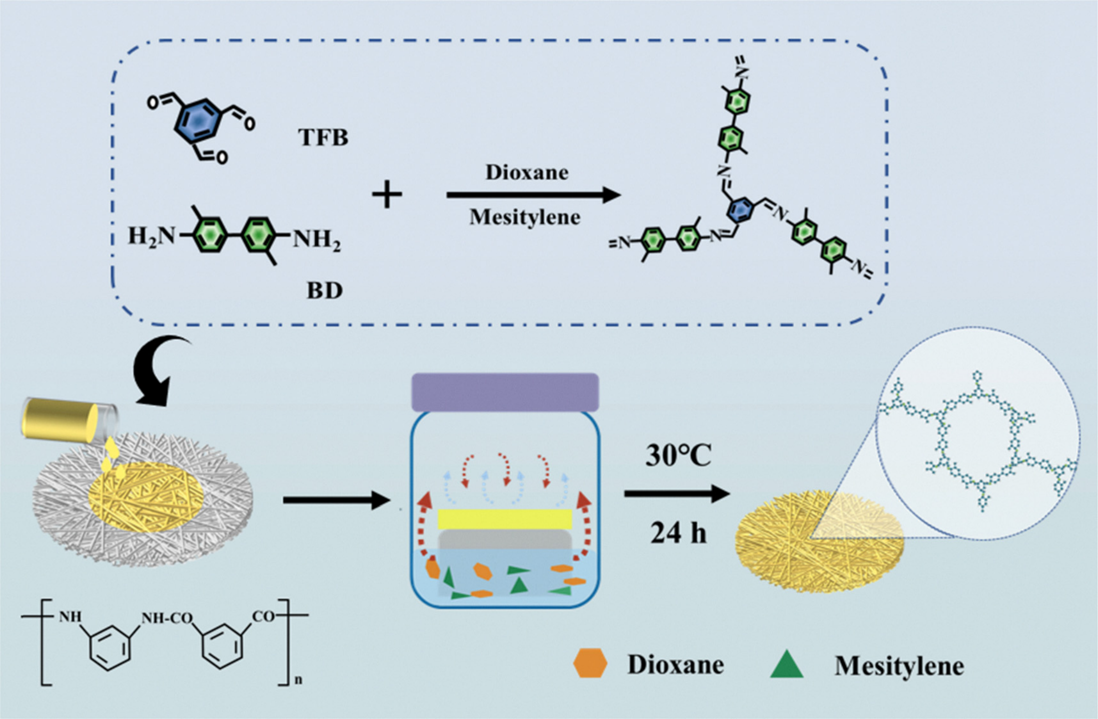

Fig. 1 Schematic of the preparation of NW-COF functional fabrics.

and the gauge between the fixtures was set to (75 ± 1) mm. The breaking strength results were the average values calculated for three samples.

2.6 Contact angle

The contact angle (CA) of the functional fabrics was measured using the Dataphysics OCA15EC Contact Angle Tester (German). A microsyringe was used to control the volume of the sessile droplet to 5 μL. The CA of NW-COF functional fabrics at different pH values (pH = 1, 3, 5, 7, 9, 11, 13) was measured. The changes in CA were measured after soaking in toluene, tetrahydrofuran, dichloromethane, methanol, acetone, acetic acid, and NaClO for 72 h, followed by washing. The CA value is calculated as the average of three droplets at different loci on the sample.

2.7 Multi-cycle stability

For the steps of the domestic washing and drying procedures for textile testing, refer GB/T 8629-2017. The samples were washed at 52 ± 1 rpm at 25 ± 2 °C for 35 min in a 1.1 g L^{-1} soap solution. Then, the samples were rinsed with tap water for 30 s, then placed in a 50 °C oven for 30 min. The tests were repeated 10 times to get the average value.

2.8 Flame retardant performance

The flame-retardant properties of functional fabrics were evaluated using a 5330 Textile Vertical Combustion Tester (Suzhou, China), in accordance with the standard GB/T 5455-2014. The continuous ignition time, smoldering time, and damage length of the sample were measured. The experimental results were the average values calculated for the three samples.

2.9 Loading

A series of NW-COF functional fabrics were prepared by the *in situ* growth of COF on NW, and the COF loading was calculated as follows,[30]

$$\omega_{\mathrm{COF}} = \frac{m_{\mathrm{COF}}}{m_{\mathrm{COF}} + m_{\mathrm{NW}}} \times 100\%$$

Herein, ω_{COF} represents the COF loading in the functional fabrics, m_{NW} represents the initial weight of NW, and m_{COF} represents the weight of the NW-COF functional fabrics.

3. Results and discussion

3.1 Characterization of COF

TFB-BD(Me)$_2$ is a typical imino COF (Fig. 2(g)), which is synthesized by the Schiff base reaction using TFB and BD(Me)$_2$ as building blocks. TFB-BD(Me)$_2$ COF can crystallize well at room temperature. SEM observations show a continuous layered topography between the COFs (Fig. 2(a)), and FTIR analysis confirms the tensile vibration of the C═N group at 1624 cm^{-1}, indicating that the Schiff base reaction proceeds smoothly (Fig. 2(b)). XRD results showed that TFB-BD(Me)$_2$ COF exhibits a high-intensity (100) reflection peak at 3.71°, mainly due to AA accumulation (Fig. 2(c)). As per the literature,[31] the effective pore size is reduced owing to the interlaminar shrinkage caused by the low-angle shift, as indicated by the XRD results. To further characterize the morphological structure of COFs, AFM analysis revealed that the diameter of the COF particles was approximately 125.3 nm (Fig. 2(e)). Nitrogen adsorption measurements were used to

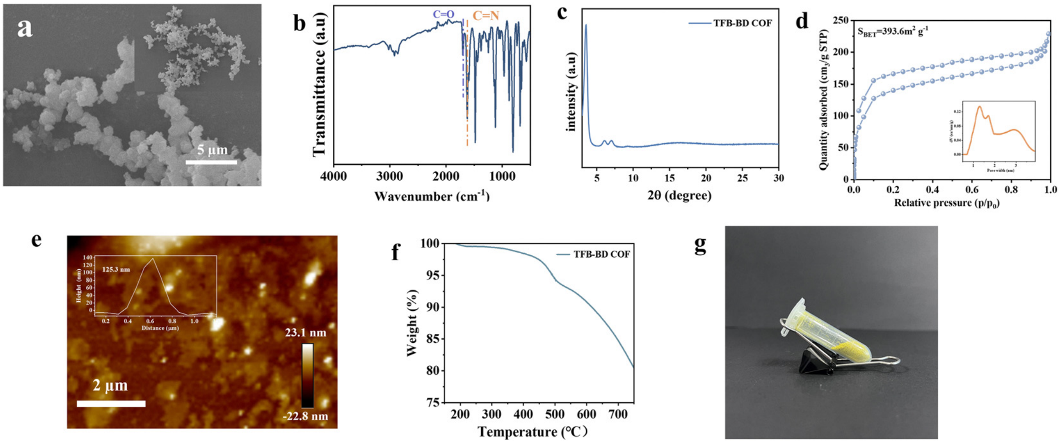

Fig. 2 (a) SEM image, (b) FTIR spectra, (c) X-ray diffraction spectra, (d) BET plot and pore size distribution plot, (e) AFM analysis, and (f) TGA of TFB-BD(Me)$_2$ COFs. (g) Schematic of TFB-BD(Me)$_2$ COFs in powder form.

determine the surface area and the specific surface area of the COF was found to be 393.6 g m^{-2}, while TFB-BD(Me)$_2$ exhibited a wider pore size distribution with a maximum at 1.3 nm (Fig. 2(d)), which was close to the predicted value based on the Eclipse AA stacking model[32,33] (theoretical value was 1.8 nm). The TGA results showed that COF had a high carbon residue rate (only 20% loss at 750 °C) and thermal stability (450 °C) at high temperatures (Fig. 2(f)), suggesting its potential flame retardant properties, however, further testing and verification are needed.

3.2 Characterization of functional fabrics

The functional fabrics prepared using COF-functionalized meta-aramid at room temperature were characterized using SEM (Fig. 3(g)). The morphology of the original NW fibers is shown in Fig. 3(a). It was found that by adjusting the content ratio of the COF precursor concentration, COF formed a continuous and uniform sheet structure and wrapped around the surface of the fiber (Fig. 3(e)). When the monomer concentration is low (TFB $<$ 0.14 mmol), a thin wrapping layer is formed on the fiber surface. Due to the low content of COF on the fiber surface, a large area of the fiber is exposed, resulting in poor hydrophobic properties of the fiber (Fig. 3(b)–(d)). However, when the monomer concentration is too high (TFB = 0.16 mmol), the additional COF particles precipitate and clog the pore size, which in turn reduces the hydrophobic properties of the functional fabrics (Fig. 3(f)).

To further evaluate the completion of the reaction, the surfaces of NW and NW-COF functional fabrics were analyzed using FTIR. It was observed that the N–H bond (3302 cm^{-1}) vibration on NW and VAC-0.14 surfaces was weakened, and the C═O peak (1646 cm^{-1}) was strongly attenuated, which indicated that TFB and BD(Me)$_2$ were successfully condensed with an imine bond (Fig. 4(a)).[34] However, FTIR is unable to unambiguously assign bond formation because the respective bands (imine: 1627 cm^{-1}, benzimidazole: 1610–1625 cm^{-1}) are in close proximity to each other to confirm the completion of the Schiff base reaction.[35–37] Therefore, we further confirmed the synthesis of NW-COF functional fabrics by XPS analysis. Fig. 4(b) shows the superimposed XPS spectra of NW and VAC-0.14. Fig. 4(c) shows that the C1s peak of the composite exhibits a migration of C═O from 287.81 eV to 288.30 eV, and the decrease in the corresponding peak content indicates the depletion of aldehyde groups during the COF reaction. This result is consistent with the literature reports.[38] With the completion of the surface Schiff base reaction, the peak content of C═N (400.63 eV) and R-NH$_2$ (398.63 eV) also increases (Fig. 4(d)). At the same time, an additional strong peak at about 3.71° was found in the XRD pattern, indicating that TFB-BD(Me)$_2$ COFs were successfully grown onto the fabric (Fig. 4(e)). TGA analysis shows that the COF layer on NW has a barrier effect, giving the functional fabrics a high thermal decomposition temperature (Fig. 4(f)). This is mainly because COFs exhibit better thermal stability during thermal decomposition, which protects the functional fabrics. The weight decay rate of VAC-0.14 is analyzed, and it is found that the weight loss rate of the prepared functional fabrics are less than 5% at 400 °C (Fig. 4(g)), which further proves that the functional fabrics have good thermal stability.

3.3 Mechanical strength

Quantitative testing of the mechanical properties of functional fabrics are shown in Fig. 5(a) and (b). The results show that the tensile strength of NW is 0.7 MPa, and the tensile properties of functional fabrics increase with the increase in COF precursor concentration. The maximum tensile strength of VAC-0.16 is 1.3 MPa. The tensile strength of the functional fabric exceeded that of the initial fabric, and its overall mechanical properties increased by 72.9%. This is attributed to the *in situ* growth of COF on the surface of the matrix, and the encapsulated state makes the interface of the composite more homogeneous.[39] More importantly, two-dimensional COF can effectively template polymer molecular chains, induce the directional arrangement of molecular chains under stress and strain-induced pore deformation, and significantly improve the damage tolerance of functional fabrics through the fiber interweaving networks. This is manifested in the improvement of breaking strength

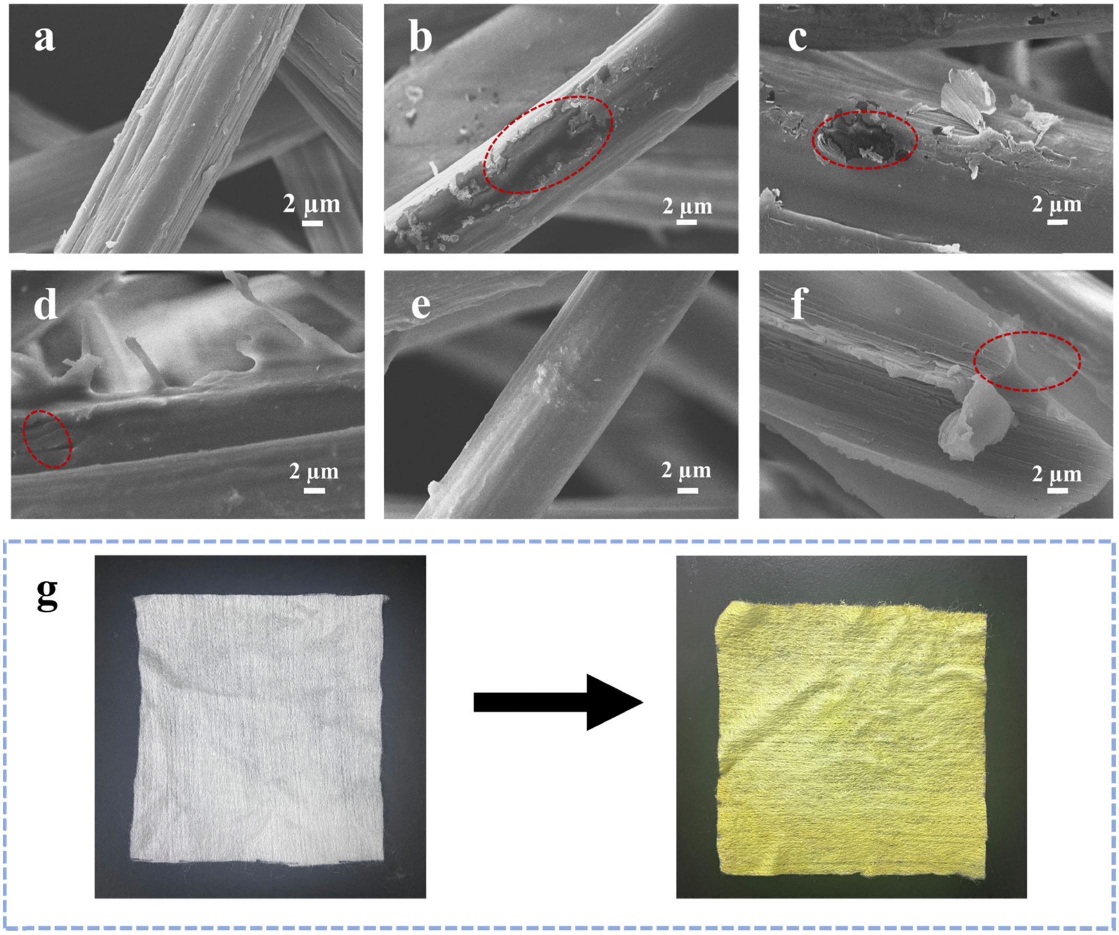

Fig. 3 SEM images of NW-COF functional fabrics, (a) NW, (b) VAC-0.02, (c) VAC-0.06, (d) VAC-0.1, (e) VAC-0.14, and (f) VAC-0.16. (g) Images of NW-COF functional fabrics before and after VAC treatment.

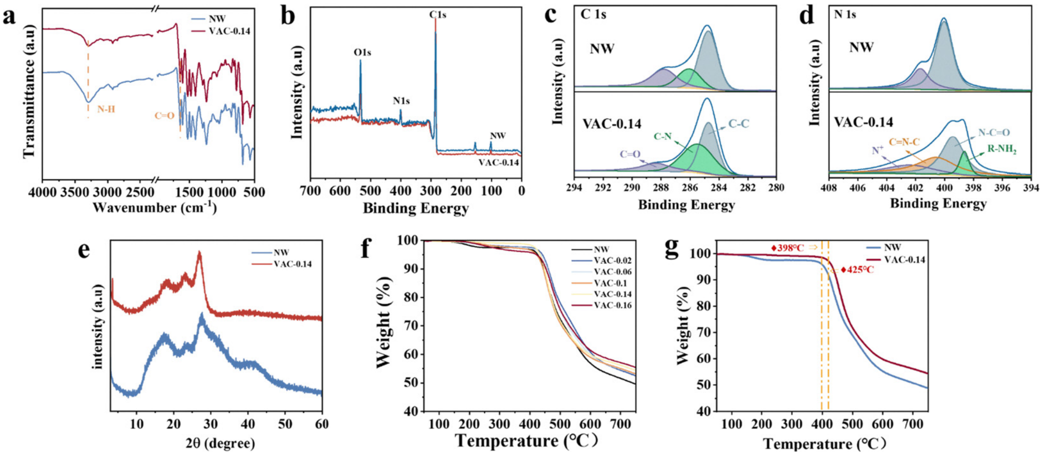

Fig. 4 (a) FTIR spectra of NW and VAC-0.14. (b) Superimposed XPS spectra of NW (blue) and VAC-0.14 (red). (c) and (d) XPS spectra, C 1s and N 1s of NW and VAC-0.14. (e) Comparison of the XRD spectra of NW and VAC-0.14. (f) and (g) Comparison of the TGA curves of NW and functional fabrics.

and toughness. From the stress–strain curve, the growth of excess COF in VAC-0.16 leads to the accumulation of energy dissipation on the fiber surface, and the uneven interaction between the matrix and the COF backbone leads to local cracks during the stretching of the functional fabric, resulting in its phased fracture[40,41] (Fig. 5(c)). The functional fabrics prepared by the vapor-assisted conversion strategy have excellent adaptability to various textile substrates and can be widely used in fibers and non-woven fabrics. In addition, the functional fabric significantly improves the chemical protection performance

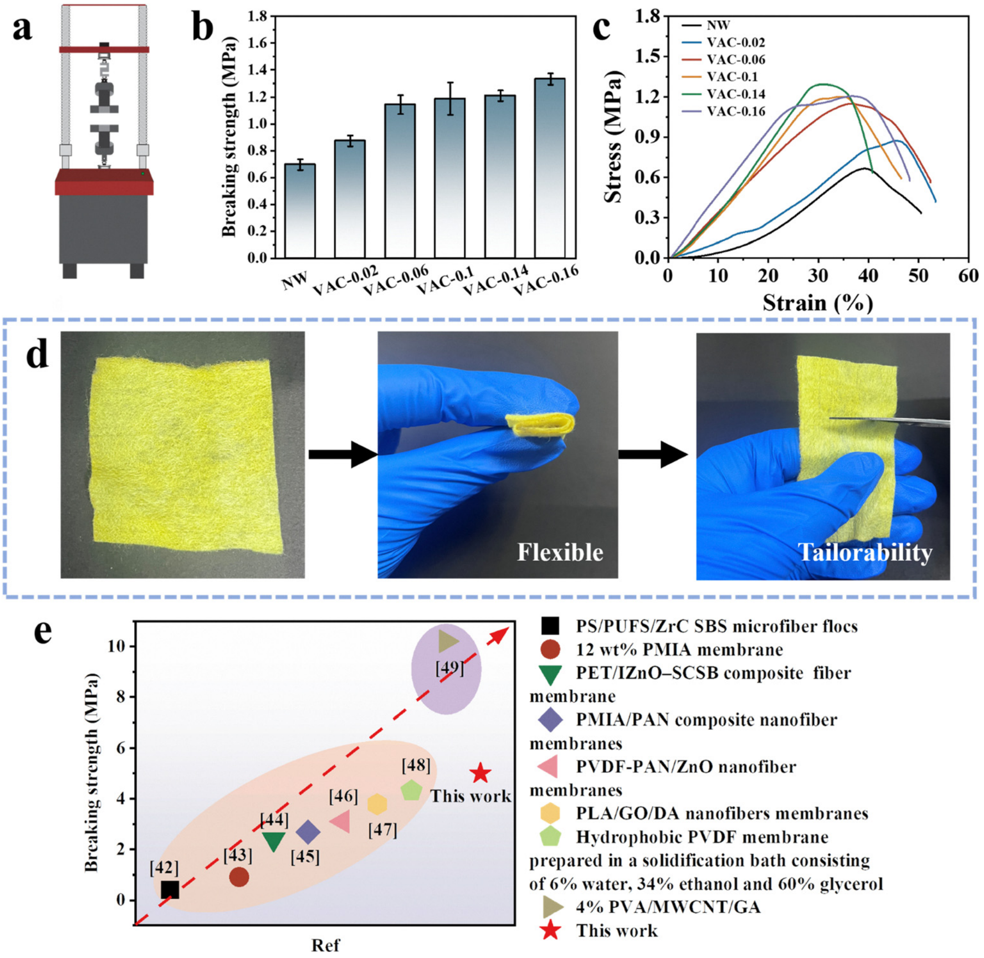

Fig. 5 (a) Diagram of the simulated equipment of the electronic tensile tester. (b) Breaking strength and (c) stress–strain curves of NW-COF functional fabrics with different concentrations. (d) Schematic of the different states of functional fabrics. (e) Comparison of the breaking strength of functional fabrics reported herein and those in the literature.

while maintaining the original properties of the non-woven (soft and cutable) (Fig. 5(d)). Fig. 5(e) summarizes the comparison of the fracture strength in this study with those reported in the literature,[42–50] indicating that the functional fabrics have specific advantages in terms of fracture strength.

3.4 Chemical barrier properties

The synergistic effect of an inert material and a chemically stable COFs imparts good hydrophobic properties to the functional fabrics. By measuring the change in water contact angle of functional fabrics, it was found that with the increase in precursor concentration, the hydrophobic contact ratio of functional fabrics also increased. VAC-0.14 has a maximum hydrophobic angle of 153° (Fig. 6(a)). This is attributed to the fact that the structure of the side-chain methyl and benzene rings in the COF chain imparts good hydrophobicity and chemical stability to COFs. Among them, too low monomer concentrations lead to discontinuous COFs coverage and insufficient exposure of hydrophobic groups on the surface of the functional fabrics, while too high monomer concentrations lead to excessive accumulation of COF, resulting in unbalanced roughness, defects and reduced hydrophobicity (Fig. 6(b)). As shown in Fig. 6(c), a large amount of COFs can be synthesized on the surface of the non-woven, with a loading rate of up to 56% for VAC-0.14 using a gas-assisted strategy. Correspondingly, the thickness of the functional fabric also gradually increased from 0.45 mm to 0.66 mm. The primary reason is that the porous, large-area non-woven fabric is used as a matrix, which provides sufficient space for the *in situ* growth of COFs. The stability of the hydrophobic properties was further evaluated by measuring the dynamic stability of the liquid on the surface of the composite fabric. The hydrophobic angle of VAC-0.14 was 150° for up to 6 min, while the hydrophobic stability of low/high concentration functional fabrics was much lower than that of VAC-0.14 (Fig. 6(d)). Methyl orange solution was sprayed on the surface of VAC-0.14, and it was found that the methyl orange solution rolled off rapidly while spraying the droplets, and the residence time on its surface was short (Fig. 6(e)). This phenomenon indicates that the adhesion between the droplets and the surface is very weak, and it has the potential for self-cleaning. In chemical protection scenarios, chemical protection fabrics can quickly repel toxic

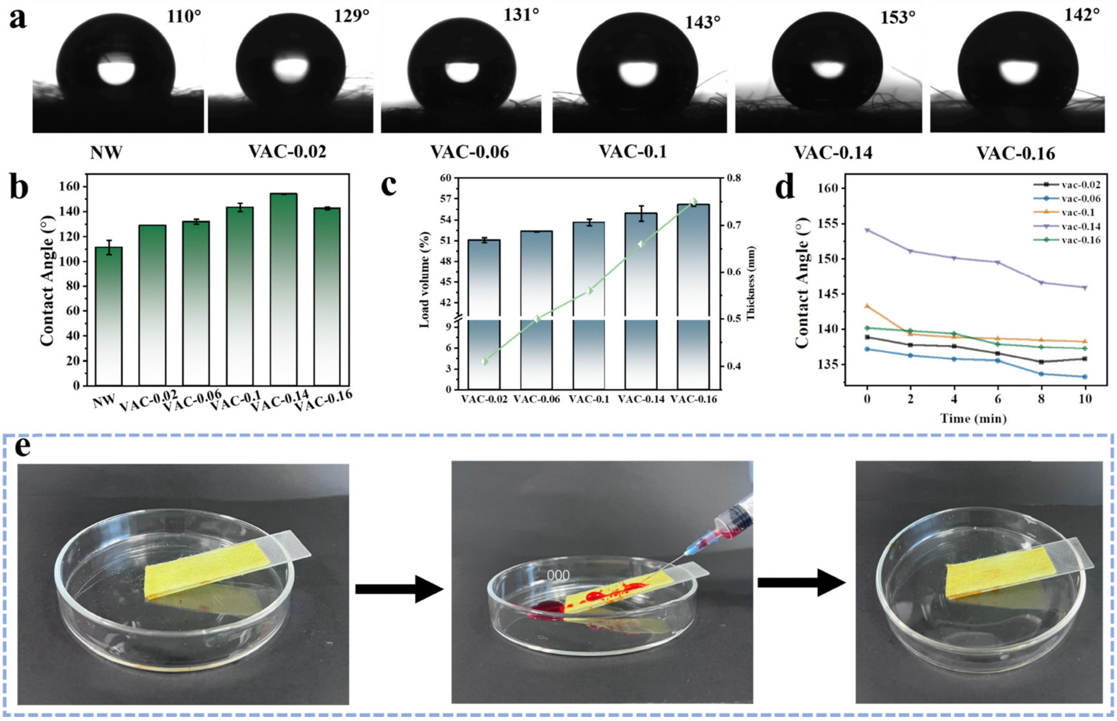

Fig. 6 (a) Photograph of the change in the water contact angle. (b) Water contact angle values at different monomer concentrations. (c) Changes in monomer loading and material thickness of different COF functional fabrics. (d) Dynamic stability map of VAC-0.14. (e) The methyl orange solution was sprayed on the surface of VAC-0.14 at high speed.

liquids (such as acids, alkalis, and organic solvents) and reduce the risk of penetration.

3.5 Chemical barrier properties

In the field of chemical protection, functional textile materials are prone to deterioration in material performance when exposed to corrosive, toxic, and harmful chemicals, which significantly affects their protective efficacy. To evaluate the chemical barrier properties of the composite fabrics, NW and VAC-0.14 were soaked in an acetic acid solution for 72 h, and the results showed that the solution quickly penetrated the NW sample and sank, whereas the VAC-0.14 sample remained floating after soaking. At the same time, FTIR showed that there was no change in the microstructure of the functional fabric after acetic acid immersion (Fig. 7(a)), which preliminarily confirmed the excellent acid corrosion resistance of the functional fabric. To further quantify its chemical barriers, the hydrophobic properties of VAC-0.14 in different chemical media were systematically determined (Fig. 7(b) and (c)). By measuring the CA of different concentrations of salt solutions and acid–base solutions with pH = 1–14 on the surface of VAC-0.14, it was found that the CA of VAC-0.14 reached a minimum of 149.9° (10% salt concentration) with increasing salt concentrations. When pH = 1, the CA of VAC-0.14 is 149.9°. With the increase in pH (acidic solution), the CA of VAC-0.14 gradually increased, and its value was 153.9° (pH = 7). As the pH continues to increase (alkaline solution), the CA of VAC-0.14 gradually decreases to a value of 147.6° (pH = 13). To further evaluate the stability and recycling performance of the chemical barrier of functional fabrics, the changes in CA of VAC-0.14 were measured after being immersed in various organic and inorganic reagents for 72 h, and it was found that the CA of functional fabrics was reduced to a minimum of 149° in acetone solution. In addition, the CA of VAC-0.14 was measured by multiple washes, and it was found that the CA of VAC-0.14 was 143.8° after 8 washes. SEM revealed no change in the fibers (Fig. 7(d) and (e)). In summary, these functional fabrics exhibit excellent chemical barrier properties as well as chemical stability. Comparison with literature[39,51–57] shows that functional fabrics have specific advantages in terms of hydrophobicity (Fig. 7(f)). However, the unique hydrophobic properties and stability of functional fabrics in multiple liquid phases give them significant advantages in different chemical environments.

3.6 Chemical protection mechanism

The chemical protection performance of functional fabrics is mainly reflected in two aspects: chemical stability of the material and its liquid phase barrier ability. Chemical stability refers to a material's ability to maintain long-term structural integrity in a chemical environment.[58] Chemical barrier performance refers to a fabric's ability to block, adsorb, or decompose harmful chemicals.[59] Studies have shown that COFs can achieve self-repair and structural reorganization of molecular backbones due to the characteristics of dynamic covalent bonds between building units, which makes COFs exhibit excellent

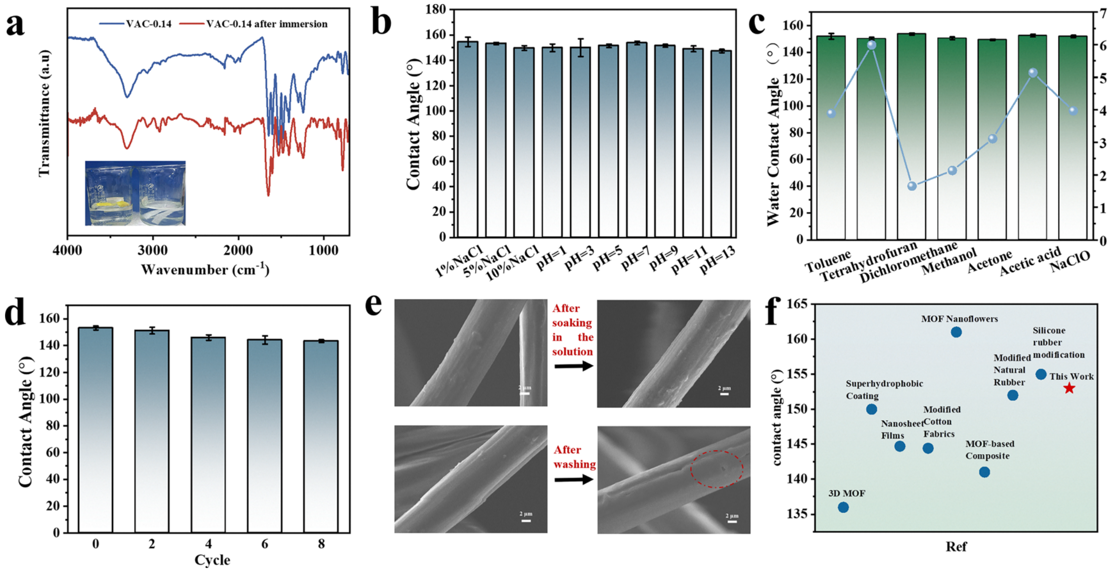

Fig. 7 (a) The FTIR and physical images of VAC-0.14 (left) and NW (right) soaked in 1 mol L^{-1} acetic acid solution for 72 h. (b) The effect of different salt concentrations and acid-alkali solutions on the contact angle of VAC-0.14 water was tested. (c) The changes in the water contact angle and weight attenuation rate of VAC-0.14 fabrics after 72 h in various organic and inorganic solutions. (d) The VAC-0.14 contact angle at different washing cycles. (e) Comparison of the SEM of NW-COF functional fabrics after solution immersion and washing. (f) Comparison of the CA in this study with those reported in the literature.

chemical stability under extreme acid–base environments and other harsh chemical conditions.[60,61] By encapsulating the COF material in the NW substrate, it not only significantly improves the overall chemical stability of the fabric but also enhances its protective performance in various liquid phase environments. The experimental results show that although NW itself is hydrophobic, in a strong acidic or alkaline environment, the simple nonwoven fabric will quickly be impregnated, resulting in a decrease in protective performance. However, the COF-modified functional fabric exhibits excellent liquid phase barrier properties owing to the hydrophobic effect of the benzene ring in the backbone and the synergistic effect of the side-chain methyl group. In addition, the reversible nature of the dynamic covalent bonds in COF ensures the structural stability and durability of the material under long-term organic solvent immersion conditions (Fig. 8).

3.7 Flame-retardant properties

In general, the combustion process of a material is mainly determined by three factors: heat, fuel, and oxygen.[62] When functional fabrics are exposed to a heat source, the combustible

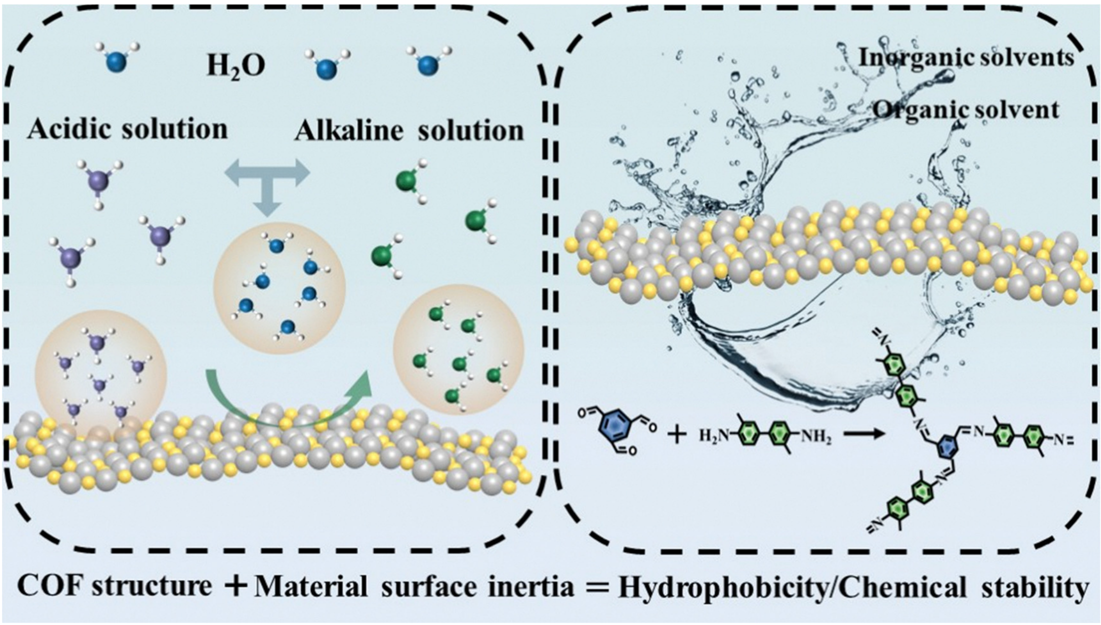

Fig. 8 Diagram showing the chemical protection mechanism.

Table 1 Comparison of the flame-retardant properties of NW-COF functional fabrics with those of NWs

Sample	Burn-up time (s)	Smoldering time (s)	Damaged length (mm)	Melting and dripping
NW	0.6	0.3	112	No
VAC-0.14	0.6	0.3	81	No

molecules in the air absorb the heat, inducing the breakage of bonds/chains to produce volatile substances and gases. In the absence of external interference, the material continues to burn until it is extinguished.[63] By testing the flame-retardant properties of the functional fabrics (Table 1), it is found that the damage length of VAC-0.14 is significantly lower than that of NW. This is because the flame retardancy of polymers is largely dependent on the response of the gas/condensed phase.[64] The intrinsic flame-retardant properties of the matrix lay the foundation for the good flame-retardant properties of functional fabrics (the burn-up time and smoldering time remain unchanged), and the COF tightly bound to the fiber surface plays the role of a protective barrier. In the condensed phase of the composite, the COF layer with a barrier effect retards the heat and mass transfer between the flame and the matrix material, hinders the dispersion of the functional fabrics from polymer to polymer, slows down the decomposition rate of the material, and ultimately reduces the combustion intensity.[65,66]

4. Conclusion

In conclusion, this study systematically demonstrates the vital application prospects of covalent organic framework materials (COFs) in the field of chemical protection composites. The results show that COF materials can significantly improve the protective performance of meta-aramid as a reinforcing phase due to their unique chemical stability and hydrophobic properties. In this study, a functionalized composite fabric system with a gradient COF concentration was successfully prepared using the vapor-assisted conversion method. The experimental results show that the functional fabrics prepared in the optimized ratio show excellent broad-spectrum chemical protection performance, as follows, it can tolerate strong acidic and alkaline environments with pH 1–14. It has a significant barrier effect on a variety of organic solvents. The mechanical properties of the material were 72.9% higher than that of the pure meta-aramid matrix. Additionally, it achieves a high COF loading rate of 56% and a superhydrophobic surface characteristic of 153°. It is worth noting that after systematic durability evaluation, including multiple wash cycles and long-term stability tests, the functional fabrics can still maintain stable hydrophobic properties and protective performance, showing excellent application potential.

Author contributions

Junmei Li, writing – original draft, conceptualization, data curation. Zhixuan Duan, software, methodology. Yinan Fan, supervision. Ruigan Zhang, visualization. Demao Ban, software. Zhaolin Liu, resources. Lifang Liu, writing – review & editing, project administration, funding acquisition.

Conflicts of interest

The authors declare that they have no known competing financial interests or personal relationships that could have appeared to influence the work reported in this paper.

Data availability

All data generated or analyzed during this study are included in this published article.

Acknowledgements

The work was supported by the ‘‘National Key R&D Program of China (2023YFC3011603)’’ and the ‘‘Taishan Industrial Experts Program (TSCX202306163)’’.

References

1 L. Hao, R. C. Shen, G. J. Liang, M. M. Kang, C. Huang, P. Zhang and X. Li, Precise local functionalization of covalent organic framework for efficient carrier separation in photocatalytic H_2 evolution, *Appl. Catal., B*, 2024, **348**, 123837.

2 B. Li, P. C. Ruan, X. Y. Xu, Z. X. He, X. Y. Zhu, L. Pan, Z. Y. Peng, Y. Y. Liu, P. Zhou, B. A. Lu, L. Dai and J. Zhou, Covalent Organic Framework with 3D Ordered Channel and Multi-Functional Groups Endows Zn Anode with Superior Stability, *Nano-Micro Lett.*, 2024, **16**, 76.

3 W. J. Yang, Y. L. Du and B. L. Liu, Novel Environmentally Friendly Covalent Organic Framework/Polylactic Acid Composite Material with High Chemical Stability for Sand-Control Material, *Polymers*, 2023, **15**, 1659.

4 Y. F. Zeng, R. Q. Zou and Y. L. Zhao, Covalent Organic Frameworks for CO_2 Capture, *Adv. Mater.*, 2016, **28**, 2855–2873.

5 Y. P. Ying, M. M. Tong, S. C. Ning, S. K. Ravi, S. B. Peh, S. C. Tan, S. J. Pennycook and D. Zhao, Ultrathin Two-Dimensional Membranes Assembled by Ionic Covalent Organic Nanosheets with Reduced Apertures for Gas Separation, *J. Am. Chem. Soc.*, 2020, **142**, 4472–4480.

6 Y. Xiao, J. Lu, K. Chen, Y. Cao, C. Gong and F.-S. Ke, Linkage Engineering in Covalent Organic Frameworks for Metal-Free Electrocatalytic C_2H_4 Production from CO_2, *Angew. Chem., Int. Ed.*, 2024, e202404738, DOI: 10.1002/anie.202404738.

7 C. Qian, A. Y. Qiu, Q. H. Huang, J. T. Liu, Q. Gao, H. W. Wu and Y. Z. Liao, Dynamic Imine Exchange Enables Access to Nanoporous Covalent Organic Frameworks with High Crystallinity for the Heck Reaction, *ACS Appl. Nano Mater.*, 2024, **7**, 9668–9677.

8 Z. M. Karazan, M. Roushani and S. J. Hoseini, Simultaneous electrochemical sensing of heavy metal ions (Zn^{2+}, Cd^{2+},

Pb^{2+}, and Hg^{2+}) in food samples using a covalent organic framework/carbon black modified glassy carbon electrode, *Food Chem.*, 2024, **442**, 138500.

9 P. Y. Zhou, Y. W. Dai, X. R. Lin, Y. X. Song, Y. F. Pang, R. Chen and R. Xiao, Specific and Magnetic Covalent Organic Framework Confined Os Nanoclusterzyme for Interference-Free and Ultrasensitive Biosensing, *Adv. Funct. Mater.*, 2024, DOI: **10.1002/adfm.202400875**.

10 X. Y. Xu, J. Zhang, Z. H. Zhang, G. D. Lu, W. Cao, N. Wang, Y. M. Xia, Q. L. Feng and S. L. Qiao, All-Covalent Organic Framework Nanofilms Assembled Lithium-Ion Capacitor to Solve the Imbalanced Charge Storage Kinetics, *Nano-Micro Lett.*, 2024, **16**, 116.

11 P. Liao, H. Ye and L. Xu, High energy capability in poly(vinylidene fluoride-*co*-chlorotrifluoroethylene) nanocomposite incorporated with Ag@polyaniline@covalent organic framework core-shell nanowire, *J. Colloid Interface Sci.*, 2024, **665**, 613–621.

12 L. H. Dai, F. Wu, Y. Xiao, Q. Liu, M. Meng, R. M. Xi and Y. M. Yin, Template-Free Self-Assembly of Hollow Microtubular Covalent Organic Frameworks for Oral Delivery of Insulin, *ACS Appl. Mater. Interfaces*, 2024, **16**, 17891–17903.

13 W. Zhang, S. Xiang, Y. X. Han, H. Y. Wang, Y. X. Deng, P. P. Bian, Y. Bando, D. Golberg and Q. H. Weng, Phospholipid-inspired alkoxylation induces crystallization and cellular uptake of luminescent COF nanocarriers, *Biomaterials*, 2024, **306**, 122503.

14 L. P. Zhai, D. D. Han, J. H. Dong, W. Q. Jiang, R. M. Nie, X. B. Yang, X. L. Luo and Z. P. Li, Constructing Stable and Porous Covalent Organic Frameworks for Efficient Iodine Vapor Capture, *Macromol. Rapid Commun.*, 2021, **42**, 2100032.

15 X. Zhang, C. Wang, Y. H. Sun, H. Ling, G. Li and X. P. Yang, Synergistically enhanced interfacial and wave-transparent properties of PBO fiber composites: Constructing self-assembly interphase with different dimensional COF, *Compos. Sci. Technol.*, 2023, **242**, 110216.

16 Y. X. Zhang, J. H. Fu, W. X. Xue, G. Q. Liu and R. L. Wu, Fluorine-Functionalized Covalent Organic Framework Superhydrophobic Modified Melamine Sponge for Efficient oil-water Separation, *Langmuir*, 2024, **40**, 6413–6423.

17 R. Wang, Y. S. Zhou, Y. Zhang, J. Xue, J. Caro and H. H. Wang, Ultrathin Covalent Organic Framework Membranes Prepared by Rapid Electrophoretic Deposition, *Adv. Mater.*, 2022, **34**, DOI: **10.1002/adma.202204894**.

18 J. Liang, Y. X. Fang, Z. L. Xu, D. Pandaya, J. Y. Dai, R. Jia and H. F. Yan, Polyester membranes with covalent organic frameworks-modified microfiltration substrate via interfacial polymerization for efficient dye nanofiltration, *Sep. Purif. Technol.*, 2024, **340**, 126757.

19 H. T. Yu, J. Y. Guan, Y. H. Chen, Y. X. Sun, S. Y. Zhou, J. F. Zheng, Q. F. Zhang, S. H. Li and S. B. Zhang, Large-Area Soluble Covalent Organic Framework Oligomer Coating for Organic Solution Nanofiltration Membranes, *Small*, 2024, **20**, DOI: **10.1002/smll.202305613**.

20 N. A. Khan, J. Q. Yuan, H. Wu, T. Huang, X. D. You, A. U. Rahman, C. S. Azad, M. A. Olson and Z. Y. Jiang, Covalent Organic Framework Nanosheets as Reactive Fillers To Fabricate Free-Standing Polyamide Membranes for Efficient Desalination, *ACS Appl. Mater. Interfaces*, 2020, **12**, 27777–27785.

21 S. E. Neumann, J. Kwon, C. Gropp, L. Ma, R. Giovine, T. Ma, N. Hanikel, K. Wang, T. Chen, S. Jagani, R. O. Ritchie, T. Xu and O. M. Yaghi, The propensity for covalent organic frameworks to template polymer entanglement, *Science*, 2024, **383**, 1337–1343.

22 H. Wang, Z. Zeng, P. Xu, L. Li, G. Zeng, R. Xiao, Z. Tang, D. Huang, L. Tang, C. Lai, D. Jiang, Y. Liu, H. Yi, L. Qin, S. Ye, X. Ren and W. Tang, Recent progress in covalent organic framework thin films: fabrications, applications and perspectives, *Chem. Soc. Rev.*, 2019, **48**, 488–516.

23 D. D. Medina, J. M. Rotter, Y. H. Hu, M. Dogru, V. Werner, F. Auras, J. T. Markiewicz, P. Knochel and T. Bein, Room Temperature Synthesis of Covalent–Organic Framework Films through Vapor-Assisted Conversion, *J. Am. Chem. Soc.*, 2015, **137**, 1016–1019.

24 Z. K. Cheng, H. Y. Wang, Z. W. Li, C. Yang, B. P. Zhang, Y. Q. Zhou, Y. X. Wang, C. Jia, L. Li and H. Wu, Processing Nomex Nanofibers by Ionic Solution Blow-Spinning for Efficient High-Temperature Exhausts Treatment, *Adv. Fiber Mater.*, 2023, **5**, 497–513.

25 S. Abbasi, M. A. Umer, M. Irfan, M. Siyar, M. Usman and M. T. Masood, Enhanced mechanical properties of surface modified and silica reinforced nomex sandwich composites, *Mater. Today Commun.*, 2023, **36**, 106346.

26 X. Yu, W. Wu, G. Xu, L. Wang, H. Yu, C.-W. Kan, J. Yan, X. Wang, Z. Wang, Y. Wu, L. Wen and Q. Zhou, Thermostable, water-repellent, moisture-permeable Nomex nanofibrous membranes with a connected PTFE network for personal protective fabrics, *Colloid Interface Sci. Commun.*, 2024, **60**, 100782.

27 N. P. Tran, C. Gunasekara, D. W. Law, S. Houshyar and S. Setunge, Repurposing of blended fabric waste for sustainable cement-based composite: Mechanical and microstructural performance, *Constr. Build. Mater.*, 2023, **362**, 129785.

28 L. Q. Shen, B. Q. Xu, H. M. Hu, Z. C. Lv and L. Ben, Facile Synthesis of Melamine/G-C_3N_4 Covalent Organic Framework (COF) by Indirect Intercalation and Its Flame Retardant, *J. Biobased Mater. Bioenergy*, 2023, **17**, 469–476.

29 Y. F. Zhou, W. Liu, W. B. Ye, S. Z. Li, F. K. Chu, W. Z. Hu, L. Song and Y. Hu, Design of ultra-microporous COF for effectively enhancing the dielectric and fire resistance of bismaleimide based electronic packaging material, *Chem. Eng. J.*, 2024, **481**, 148409.

30 Q. Li, Q. Liu, J. Zhao, Y. Hua, J. Sun, J. Duan and W. Jin, High efficient water/ethanol separation by a mixed matrix membrane incorporating MOF filler with high water adsorption capacity, *J. Membr. Sci.*, 2017, **544**, 68–78.

31 L. Chen, C. Zhou, H. Yang, J. Lin, Y. Ge, W. Zhou, C. Lu, L. Tan and L. Dong, Room-temperature fabrication of superhydrophobic covalent organic framework (COF) decorated cotton fabric for high-flux water-in-oil emulsion separation, *Chem. Commun.*, 2021, **57**, 11533–11536.

32 Z. Alsudairy, N. Brown, C. Yang, S. Cai, F. Akram, A. Ambus, C. Ingram and X. Li, Facile Microwave-Assisted Synthesis of 2D Imine-Linked Covalent Organic Frameworks for Exceptional Iodine Capture, *Precis. Chem.*, 2023, **1**, 233–240.

33 E. Dautzenberg, M. Lam, G. Li and L. C. P. M. de Smet, Enhanced surface area and reduced pore collapse of methylated, imine-linked covalent organic frameworks, *Nanoscale*, 2021, **13**, 19446–19452.

34 J.-X. Guo, H.-L. Qian, X. Zhao, C. Yang and X.-P. Yan, In situ room-temperature fabrication of a covalent organic framework and its bonded fiber for solid-phase microextraction of polychlorinated biphenyls in aquatic products, *J. Mater. Chem. A*, 2019, **7**, 13249–13255.

35 L. Sun, M. Yang, H. Guo, T. T. Zhang, N. Wu, M. Y. Wang, F. Yang, J. Y. Zhang and W. Yang, COOH-MWCNT connected COF and chemical activated CTF as a novel electrochemical sensing platform for simultaneous detection of acetaminophen and *p*-aminophenol, *Colloids Surf., A*, 2022, **647**, 129092.

36 E. Dautzenberg, G. N. Li and L. De Smet, Aromatic Amine-Functionalized Covalent Organic Frameworks (COFs) for CO_2/N_2 Separation, *ACS Appl. Mater. Interfaces*, 2023, DOI: 10.1021/acsami.2c17672.

37 M. G. Rabbani and H. M. El-Kaderi, Template-Free Synthesis of a Highly Porous Benzimidazole-Linked Polymer for CO_2 Capture and H_2 Storage, *Chem. Mater.*, 2011, **23**, 1650–1653.

38 E. Dautzenberg, G. Li and L. C. P. M. de Smet, Aromatic Amine-Functionalized Covalent Organic Frameworks (COFs) for CO_2/N_2 Separation, *ACS Appl. Mater. Interfaces*, 2023, **15**, 5118–5127.

39 Y. Ma, Y. Wang, H. Li, X. Guan, B. Li, M. Xue, Y. Yan, V. Valtchev, S. Qiu and Q. Fang, Three-Dimensional Chemically Stable Covalent Organic Frameworks through Hydrophobic Engineering, *Angew. Chem., Int. Ed.*, 2020, **59**, 19633–19638.

40 J. Choi, C. M. Hui, J. Pietrasik, H. Dong, K. Matyjaszewski and M. R. Bockstaller, Toughening fragile matter: mechanical properties of particle solids assembled from polymer-grafted hybrid particles synthesized by ATRP, *Soft Matter*, 2012, **8**, 4072–4082.

41 A. T. Ngo, J. Richardi and M. P. Pileni, Cracks in Magnetic Nanocrystal Films: Do Directional and Isotropic Crack Patterns Follow the Same Scaling Law?, *Nano Lett.*, 2008, **8**, 2485–2489.

42 Y. Liu, J. Zheng, X. Zhang, Y. Du, G. Yu, K. Li, Y. Jia and Y. Zhang, Hyperbranched polyamide modified graphene oxide-reinforced polyurethane nanocomposites with enhanced mechanical properties, *RSC Adv.*, 2021, **11**, 14484–14494.

43 F. Liu, Y. Liang, H. Xiang, W. Li, H. Liang, W. Shao, X. Li, P. Han, J. He and Z. Yuan, Stretchable and ultra-light nonwoven thermal material with effective photo-thermal conversion based on solution blow spinning technology, *J. Appl. Polym. Sci.*, 2024, **141**, e54940.

44 J. Yu, X. Tian, B. Xin and J. Xu, Preparation and Characterization of PMIA Nanofiber Filter Membrane for Air Filter, *Fibers Polym.*, 2021, **22**, 2413–2423.

45 L. Yu, D. Liu, P. Gu, K. Chen and H. Qiu, PET Composite Fiber Membranes Modified with Modified Nanoscale ZnO Exhibit Synergistic Antibacterial Effects, *Fibers Polym.*, 2023, **24**, 3947–3960.

46 H. Zhang, Y. Xie, Y. Song and X. Qin, Preparation of high-temperature resistant poly(*m*-phenylene isophthalamide)/polyacrylonitrile composite nanofibers membrane for air filtration, *Colloids Surf., A*, 2021, **624**, 126831.

47 A. K. Assaifan, M. O. Aijaz, M. Luqman, Q. A. Drmosh, M. R. Karim and H. F. Alharbi, Removal of cadmium ions from water using coaxially electrospun PAN/ZnO-encapsulated PVDF nanofiber membranes, *Polym. Bull.*, 2022, **79**, 2831–2850.

48 T. Zhu, L. Zhao, M. Qian, D. Yu, J. He, W. Jiang, J. Wang and S. Wang, Biomimetic electrospinning for fabrication of poly(lactic acid)/graphite oxide/poly(dopamine) nanofiber membrane, *J. Eng. Fibers Fabr.*, 2023, **18**, 15589250231181912.

49 Z. Fan, M. Hu, K. Hou, K. Jin, H. Zhao and Z. Cai, Fabrication of Hydrophobic Poly(vinylidene fluoride) Membranes with Manipulated Micromorphology and Enhanced Strength, *Langmuir*, 2023, **39**, 8629–8637.

50 L. Fan, X. Mei, J. Zhang, J. Zhu, X. Wang, Y. Li and W. Cai, Effect of multi-walled carbon nanotube on thermal decomposition, mechanical and heat-induced shape memory properties of crosslinked poly(vinyl alcohol), *Smart Mater. Struct.*, 2021, **30**, 115017.

51 W. Zhu, Y. Xu, J. He and X. Dong, Transparent Superhydrophobic Coatings with Mechanical and Chemical Stability Prepared by Modified Polyhedral Oligosilsesquioxanes via UV-Curable Method, *Coatings*, 2023, **13**, 498.

52 L. Yang, C. Yao, R. Wang, L. Jiang, W. Zhu, M. Wang, L. Liu, D. Liang, L. Hu, C. Den, Q. Yin, M. Zhang, G. He, J. Lv and Z. Sun, Novel $Fe_2O_3/\{101\}TiO_2$ nanosheet array films with stable hydrophobicity and enhanced photoelectrochemical performance, *Mater. Chem. Phys.*, 2022, **275**, 125226.

53 S. Nie, D. Jin, J.-N. Yang, G. Dai and Y. Luo, Fabrication of environmentally-benign flame retardant cotton fabrics with hydrophobicity by a facile chemical modification, *Cellulose*, 2019, **26**, 5147–5158.

54 N. Ahmad, S. Rasheed, T. Ali, I. Azhar, W. Ahmad and D. Hussain, Superoleophilic cotton fabric decorated with hydrophobic Zn/Zr MOF nanoflowers for efficient self-cleaning, UV-blocking, and oil–water separation, *Chem. Eng. J.*, 2024, **485**, 149991.

55 S. Ghosh, A. Rana, S. Kumar, C. Gogoi, S. Mukherjee, U. Manna and S. Biswas, A self-cleaning hydrophobic MOF-based composite for highly efficient and recyclable separation of oil from water and emulsions, *Mater. Chem. Front.*, 2022, **6**, 2051–2060.

56 S. N. Dissanayake, K. De Silva, S. M. Egodage, F. D. Blum and M. Maddumaarachchi, Enhancement of hydrophobicity in natural rubber vulcanizates using diatomaceous earth, *Prog. Rubber Plast. Recycl. Technol.*, 2023, 14777606231224129, DOI: 10.1177/14777606231224129.

57 R. Han, Z. Han, X. Song, W. Cui, J. Peng, G. Dong and K. Niu, Hydrophilic silica transformed silicone rubber into

Superhydrophobic composites, *Polym. Compos.*, 2024, **45**, 873–881.

58 H. Furukawa, F. Gándara, Y.-B. Zhang, J. Jiang, W. L. Queen, M. R. Hudson and O. M. Yaghi, Water Adsorption in Porous Metal–Organic Frameworks and Related Materials, *J. Am. Chem. Soc.*, 2014, **136**, 4369–4381.

59 Q. Sun, B. Aguila, J. A. Perman, T. Butts, F.-S. Xiao and S. Ma, Integrating Superwettability within Covalent Organic Frameworks for Functional Coating, *Chem*, 2018, **4**, 1726–1739.

60 K. Geng, T. He, R. Liu, S. Dalapati, K. T. Tan, Z. Li, S. Tao, Y. Gong, Q. Jiang and D. Jiang, Covalent Organic Frameworks: Design, Synthesis, and Functions, *Chem. Rev.*, 2020, **120**, 8814–8933.

61 R. Gavara, S. Royuela and F. Zamora, A minireview on covalent organic frameworks as stationary phases in chromatography, *Front. Chem.*, 2024, **12**, 1384025.

62 L.-Y. Lv, C.-F. Cao, Y.-X. Qu, G.-D. Zhang, L. Zhao, K. Cao, P. Song and L.-C. Tang, Smart fire-warning materials and sensors: Design principle, performances, and applications, *Mater. Sci. Eng., R*, 2022, **150**, 100690.

63 D. K. Chattopadhyay and D. C. Webster, Thermal stability and flame retardancy of polyurethanes, *Prog. Polym. Sci.*, 2009, **34**, 1068–1133.

64 L. Zhang, Z. Li and D.-Y. Wang, Polydopamine-assisted strategies for preparation of fire-safe polymeric materials: A review, *Eur. Polym. J.*, 2020, **138**, 109973.

65 X.-H. Shi, X.-L. Li, Y.-M. Li, Z. Li and D.-Y. Wang, Flame-retardant strategy and mechanism of fiber reinforced polymeric composite: A review, *Composites, Part B*, 2022, **233**, 109663.

66 C. K. Kundu, Z. Li, L. Song and Y. Hu, An overview of fire retardant treatments for synthetic textiles: From traditional approaches to recent applications, *Eur. Polym. J.*, 2020, **137**, 109911.